Research Article Vol. 10, No. 3 / March 2022 / Photonics Research 637

PHOTONICS Research

Sub-50 fs pulses at 2050 nm from a picosecond Ho:YLF laser using a two-stage Kagome-fiber-based compressor

Krishna Murari,[1,2,3,*] Giovanni Cirmi,[1,4] Hüseyin Cankaya,[1,4] Gregory J. Stein,[1] Benoit Debord,[5] Frederic Gérôme,[5] Felix Ritzkosky,[1] Fetah Benabid,[5] and Franz X. Kärtner[1,2,4]

[1]Center for Free Electron Laser Science CFEL, Deutsches Elektronen-Synchrotron DESY, 22607 Hamburg, Germany
[2]Max-Planck Institute for Structure and Dynamics of Matter (MPSD), 22761 Hamburg, Germany
[3]ELI-ALPS, ELI-HU Non-Profit Ltd., Szeged H-6728, Hungary
[4]The Hamburg Center for Ultrafast Imaging & Department of Physics, University of Hamburg, 22761 Hamburg, Germany
[5]GPPMM Group, XLIM Research Institute, UMR 7252 CNRS, University of Limoges, Limoges, France
*Corresponding author: krishna.murari@desy.de

Received 30 August 2021; revised 6 January 2022; accepted 7 January 2022; posted 7 January 2022 (Doc. ID 441674); published 9 February 2022

The high-energy few-cycle mid-infrared laser pulse beyond 2 μm is of immense importance for attosecond science and strong-field physics. However, the limited gain bandwidth of laser crystals such as Ho:YLF and Ho:YAG allows the generation of picosecond (ps) long pulses and, hence, makes it challenging to generate few-cycle pulse at 2 μm without utilizing an optical parametric chirped-pulse amplifier (OPCPA). Moreover, the exclusive use of the near-infrared wavelength has limited the generation of wavelengths beyond 4 μm (OPCPA). Furthermore, high harmonic generation (HHG) conversion efficiency reduces dramatically when driven by a long-wavelength laser. Novel schemes such as multi-color HHG have been proposed to enhance the harmonic flux. Therefore, it is highly desirable to generate few-cycle to femtosecond pulses from a 2 μm laser for driving these experiments. Here, we utilize two-stage nonlinear spectral broadening and pulse compression based on the Kagome-type hollow-core photonic crystal fiber (HC-PCF) to compress few-ps pulses to sub-50 fs from a Ho:YLF amplifier at 2 μm at 1 kHz repetition rate. We demonstrate both experimentally and numerically the compression of 3.3 ps at 140 μJ pulses to 48 fs at 11 μJ with focal intensity reaching 10^{13} W/cm^2. Thereby, this system can be used for driving HHG in solids at 2 μm. In the first stage, the pulses are spectrally broadened in Kagome fiber and compressed in a silicon-based prism compressor to 285 fs at a pulse energy of 90 μJ. In the second stage, the 285 fs pulse is self-compressed in air-filled HC-PCF. With fine-tuning of the group delay dispersion (GDD) externally in a 3 mm window, a compressed pulse of 48 fs is achieved. This leads to a 70-fold compression of the ps pulses at 2050 nm. We further used the sub-50 fs laser pulses to generate white light by focusing the pulse into a thin medium of YAG.

https://doi.org/10.1364/PRJ.441674

1. INTRODUCTION

High-energy ultrashort mid-infrared (mid-IR) laser radiation is of vast importance due to its wide applications ranging from spectroscopy [1] and high-speed electronics to attoscience phenomena and strong-field physics. Tabletop attosecond light sources rely on high harmonic generation (HHG) when a few-cycle intense laser pulse interacts with noble gases in vacuum. Until now, Ti:sapphire lasers centered at 800 nm have been the major workhorse for driving the HHG to generate isolated attosecond pulses in 10s of eV range. Scaling of the photon energies by HHG beyond 100 eV or to the keV range requires the development of high-energy few-cycle lasers at longer wavelengths for driving the HHG process. It is well known that the cutoff energy of the HHG scales quadratically with the wavelength according to $\hbar\varpi = I_p + 3.17U_p$, where U_p is the ponderomotive energy $U_p \propto I_p\lambda^2$. Furthermore, long-wavelength lasers permit the study of electron acceleration in the dielectric structures and plasmas [2], breakdown of the dipole approximation [3], and rotational/vibrational spectroscopy [4]. Besides, they are an ideal tool to investigate non-perturbative strong-field effects in solids such as the dynamical Frantz–Keldysh effect [5,6] and high-order harmonics from Bloch oscillations [7,8]. The recent development of few-cycle lasers in the range 1.6–2.1 μm has led to the generation of harmonics up to 0.5 keV [9–11]. However, the conversion efficiency of HHG reduces dramatically with the increase in the

driving wavelength owing to the quantum diffusion effects of the electronic wave packets [12], thereby reducing the total flux of the attosecond pulses. Hence, innovative schemes are utilized to achieve useful photon flux to be able to use it for the attosecond experiments when driven by the long-wavelength lasers. It is suggested that the usage of multi-color fields for driving the HHG can efficiently enhance the harmonic yield [13–15]. When the HHG process is driven with a combination of a strong infrared (IR) and a weak XUV/VUV pulse train with typical intensities of 10^{14} W/cm^2 and 10^{13} W/cm^2, respectively, the harmonic signal in the plateau region can be enhanced significantly by 2–3 orders of magnitude [16,17]. For instance, it has been shown numerically, when a strong 2 μm pulse is seeded by a 10× weaker pulse at 400 nm, the harmonic yield is enhanced in the 100–400 eV range [18]. Furthermore, carrier-envelope phase (CEP) stability is crucial in these experiments, and it is desired that the two fields be generated from the same laser front-end to be able to control the time delay between the two pulses. However, it is challenging to generate such an intense pulse for both long mid-IR (4–10 μm) and near-IR pulse from the same front-end laser.

Generation of an intense few-cycle mid-IR pulse is achieved using the optical parametric amplifier (OPA) or optical parametric chirped-pulse amplifier (OPCPA). When properly scaling the pulse energy to the multi-mJ level, they even permit the realization of bright coherent table-top HHG sources in the water-window and keV X-ray region [19,20]. However, access to long wavelengths beyond 4 μm is limited, as the pump source of these OPCPA relies mostly on the near-IR wavelength at 800 nm or 1 μm. This is mainly due to the use of oxide crystals for frequency conversion that are not transparent beyond 4 μm and low quantum efficiency due to unfavorable quantum defects at the longer wavelength. Non-oxide crystals such as ZGP, $CdSiP_2$, or OP-GaAs capable of generating longer mid-IR pulses require pumping above 1.9 μm for better phase matching and higher conversion efficiency [21,22]. Hence, 2 μm laser pulses with mJ-level energy are highly desirable for pumping of the non-oxide nonlinear crystals and preferably with sub-ps pulse duration to generate stable and coherent white light continua for seeding the OPA featuring self-CEP-stabilization of the idler [23]. Unfortunately, though most of the 2 μm laser gain media such as Tm- or Ho-based crystals can generate pulses with high energy, they suffer from very narrow gain bandwidth, which further reduces due to gain narrowing (GN) during the amplification, that leads to several ps-long output pulses after amplification in the CPA schemes. Hence, novel schemes are needed to compress the pulses to the few-cycle regime.

The commonly used approach to broaden the output spectrum from a CPA laser is nonlinear spectral broadening in waveguides followed by dispersion compensation. When an intense ultrashort laser pulse propagates in an optical waveguide, it gives rise to several intensity-dependent nonlinear effects such as self-phase modulation (SPM), stimulated Raman scattering (SRS), and four-wave mixing (FWM). These processes give rise to new frequencies, and with proper dispersion management, pulses shorter than the input are generated. Nonlinear pulse compression can be implemented in several schemes such as in bulk dielectric media [24,25], a multi-pass gas cell [26,27], or a hollow-core waveguide [28,29], but each of them has its limitation; hence, their usage relies on the application. For instance, broadening in bulk media suffers from modal instabilities and pulse breakup at high energies. Nonlinear spectral broadening in noble gas-filled hollow-core capillary fiber (HCF) and dispersion management externally achieved a breakthrough with the invention of chirp mirrors [30], which allowed compact and precise control of dispersion. It is noteworthy that the HCF consists of a glass capillary, not to be confused with an optical fiber. Since then, large-core diameter HCFs are routinely used to generate few-cycle pulses at 800 nm with pulse energies in mJ range. However, their large core structure leads to high bending loss, thereby requiring the fiber to be kept straight for the entire length of the fiber and making them highly prone to the environmental conditions. In addition, they have a very low transmission efficiency (∼50%) that restricts the beam to propagate to long distances in the fiber. Furthermore, the critical intensity needed to initiate the spectral broadening is high; therefore, it cannot be used for systems with low pulse energy or long picosecond (ps) systems. In contrast, hollow-core photonic crystal fiber (HC-PCF) offers much higher power delivery capability with significantly lower transmission loss and broad transmission bandwidth [31]. There exist two main types of HC-PCFs, mainly based on either photonic bandgap (PBG) or inhibited coupling (IC) [32]. Though PBG-based HC-PCFs offer low transmission loss, they suffer from low damage threshold, due to the large core-cladding mode overlap. On the other hand, the emergence of negative-curvature core boundary HC-PCF (Kagome) [33], due to its mode propagation phenomena of IC, offers lower power overlap between the core and cladding, leading to a much higher damage threshold. In these fibers, the negative contour enhances the coupling-inhibition of the core-guided optical modes to the cladding, thanks to a stronger transverse mismatch between the core mode and the cladding modes, and to a lower spatial overlap with the cladding strut nodes [34]. As a result, these fibers can offer enlarged core diameter, low group delay dispersion (GDD), broad transmission bandwidth, and long length for beam delivery [33,34]. Apart from record pulse energy handling capacity and compression [35,36], these fibers also support, when filled with the appropriate gas, a variety of nonlinear optical interactions like Raman scattering [37] and extreme nonlinear phenomena like HHG [38,39], which makes them attractive to study nonlinear pulse propagation in the presence of noble gases.

In recent years, nonlinear compression in Kagome fiber at 800 nm or 1030 nm wavelengths [40,41] has seen rapid progress for both high-energy [36,42] and high-average-power systems [43]. Very few self-compression experiments have been demonstrated at wavelengths near 2 μm with the input pulse duration ranging from a few 10s to a few 100s of fs. Balciunas *et al.* achieved remarkable self-compression of 80 fs pulses down to the single-cycle limit at 1.8 μm with output pulse energies of 25 μJ [44]. Moreover, regardless of the pump wavelength, compression of pulses starting from ps duration is extremely challenging and has been rarely reported. There exist few demonstrations with an input pulse duration of 6 ps [45] and 27 ps

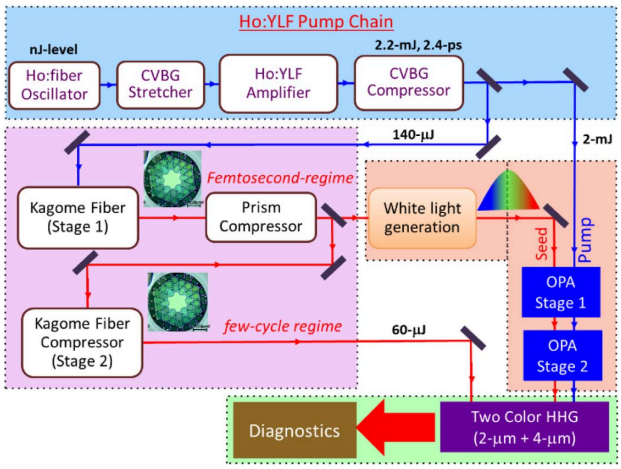

Fig. 1. Proposed scheme of two-color HHG driven by Ho-CPA as front-end.

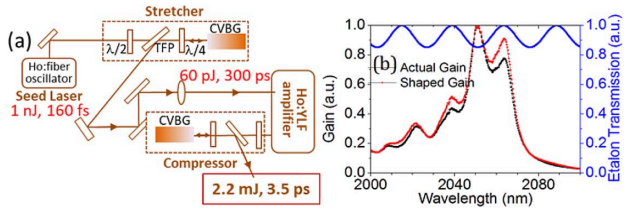

Fig. 2. (a) The schematic layout of the Ho-CPA based on Ho:fiber oscillator, amplifier, and chirp volume Bragg grating (CVBG)-based stretcher and compressor with half-wave plate ($\lambda/2$), quarter-wave plate ($\lambda/4$), and thin-film polarizer (TFP). (b) The principle of intracavity gain shaping using an etalon in the amplifier: the etalon transmission (blue) aligned with the gain spectrum (black) that yields effectively broader net gain spectrum (red).

[46] at 1030 nm, but the main goal of these experiments was rather different and geared toward Raman scattering instead of pulse compression. First, picosecond compression at 2 μm wavelength was demonstrated by Murari *et al.* by compressing 3.3 ps pulses to 285 fs [47]. Here, we present generation of sub-50 fs pulses from the ps output of a Ho:YLF-based chirped pulse amplifier (Ho-CPA) system at 2 μm by utilizing two-stage nonlinear compression. This simple, compact, and robust high-energy system at 2 μm can serve as a laser driver for HHG in solids and it enables passively CEP stable idler wave for the two-color HHG experiments as shown in Fig. 1. The pump chain consists of a Ho-fiber oscillator, Ho:YLF regenerative amplifier (RA), and chirp volume Bragg grating (CVBG) for pulse stretching and compression. The Ho-CPA operates at a 1 kHz repetition rate, and a small portion energy of 140 μJ is sent into a two-stage nonlinear compressor; the remaining energy of ∼2 mJ can be used for pumping ZGP-based OPA. In two stages, the ps pulse is compressed to sub-50 fs. The intensity of the few-cycle output of the second stage reaches peak intensity of $\sim 10^{13}$ W/cm^2. Furthermore, we generate white light by focusing the output from the second stage into a thin YAG window for seeding ZGP-based OPA. Hence, the idler output of the OPA at 4 μm can act as a weak pulse for two-color HHG. This method to obtain few-cycle pulses at 2 μm opens a route toward a compact and robust source for driving HHG in solids at mid-IR and two-color HHG for enhanced attosecond flux. Furthermore, it also offers a stable compact and stand-alone laser source for broadband supercontinuum generation, which has numerous applications in spectroscopy and metrology.

2. EXPERIMENTAL SETUP

A. Ho:YLF Laser Amplifier

The high-energy picosecond pump pulses are derived from Ho-CPA with a homebuilt Ho-fiber oscillator and a commercial Ho:YLF RA from Q-Peak Inc. The schematic of the laser source is depicted in Fig. 2. The Ho-fiber oscillator emits pulses at 34 MHz repetition rate with a pulse energy of 1 nJ and a duration of 160 fs. The output spectrum is centered at 2060 nm with a spectral bandwidth of 37 nm full width at half-maximum (FWHM). The oscillator pulses are stretched in a CVBG from OptiGrate Inc. to 300 ps, and due to the filtering effect in CVBG, the seed bandwidth before amplification reduces to 8.2 nm FWHM. The stretched pulses are amplified in the RA and a single-pass booster both based on Ho:YLF crystals, which are end-pumped by a Tm-fiber laser at 1940 nm. After amplification, the spectral bandwidth of the output spectrum reduces from 8.2 nm to 2.3 nm, which is compressed using the same CVBG as used for stretching. At the output, the pulse energy of 2.2 mJ with the duration of 3.5 ps FWHM is achieved. However, we found that this pulse duration was somewhat longer than that required for suppressing pulse break in the first Kagome fiber compressor as described in the next subsection. Therefore, we explored a method to shorten the pulse duration of the output pulse from the Ho-CPA system by mitigating the gain-narrowing (GN) effect in the RA.

To reduce the GN-effect during the amplification in the RA, we insert an optimized etalon inside the RA cavity. The etalon acts as an anti-GN frequency-selective filter that enhances the output spectrum, leading to the shortening of the pulse duration. An etalon has a sinusoidal transmission function whose period depends on thickness, the modulation depth depends on reflectivity, and the phase depends on the angle of incidence. Hence, by careful choice of thickness, reflectivity and phase of the etalon, the effect of GN after each round trip is reduced thereby increasing the effective output spectrum. The angle of the etalon is tuned in such a way that its transmission minimum is aligned with the gain maximum. With the use of fused silica etalon of thickness 290 μm and reflectivity 3.3%, the spectral bandwidth is increased from 2.9 nm to 5.4 nm. The complete optimization of the gain shaping using an etalon can be found in Ref. [48]. After etalon optimization, the Ho-CPA is operated at a lower pulse energy of 1.7 mJ with a pulse duration of 3.3 ps (without etalon) and 1.8 ps (with etalon).

B. Dual-Stage Kagome-Fiber-Based Compressor

Our nonlinear dual-stage compressor consists of Kagome fiber based on a hypocycloid-core-contour (7-cell and 19-cell) specially designed for operation at 2-μm wavelength in the

anomalous dispersion regime. The fiber is fabricated by the GPPMM group in France. The 7-cell fiber has an inner core diameter of 63 μm with mode field diameter (MFD) of 44 μm and NA of 0.018 while the 19-cell fiber has an inner core diameter of 82 μm, MFD of 54 μm, and NA of 0.014. It also has a very broad transmission range of 400–2400 nm and exhibits a relatively low propagation loss of 0.2 dB/m at 2 μm. The calculated group velocity dispersion (GVD) of the fiber at 2 μm is low and anomalous with a value of −2200 fs^2/m, and, hence offers the possibility of pulse self-compression that occurs due to the interplay between the SPM and GVD [47].

We initially launched the pulses in a 19-cell fiber with a length of 3.5 m and high-energy up to 780 μJ at 3.3 ps duration. From the exit end of the fiber, inert gas Ar at a pressure of 3 bar is injected. Figure 3(a) shows the waterfall plots of spectral broadening obtained at the output of the fiber with increasing input energy from 85 μJ to 780 μJ beyond which fiber damage is observed. The spectrum is measured using the NIRQuest grating spectrometer from Ocean Optics Inc. that has high resolution of 1.5 nm and spectral range from 1850 to 2150 nm. As the energy is increased, the pulse encounters very limited broadening due to the generation of the high order soliton leading to soliton fission. Due to the ps-long input pulse the soliton order N is very high and thus leads to pulse breakup and the input energy is transferred to many sub-pulses instead of broadening the spectrum of the fundamental pulse. The red-dashed line shown in the Fig. 3(a) demonstrates the fissioned solitons at the longer wavelength than the pump as the input energy increased. Hence, it is important to reduce the pulse duration from the amplifier output before launching into the nonlinear fiber compressor. This is achieved by employing a spectral filter such as an etalon to mitigate the GN effect in the RA (as described in the previous section). After shortening of the pulse by intracavity spectral shaping, the 1.8 ps pulse from the amplifier is re-launched into the 19-cell fiber with the same length as before, and the spectrum is measured with increasing pulse energy from 99 μJ to 709 μJ. The results are plotted as waterfall plots in Fig. 3(b). In this case, at the highest energy of 709 μJ, the broadened spectral width at 10 dB is 77 nm. It is evident from Fig. 3 that the required broadening can be achieved by reducing the input pulse duration from 3.3 ps to 1.8 ps; hence, no pulse breakup is observed. In addition, it is also worth noting from Fig. 3 (right) that the bandwidth $\Delta\lambda$ of 77 nm is achieved with an input energy of 709 μJ. However, driven by the goal to send only a small portion of the pulse energy from the main amplifier to the post-compression to be able to pump the OPA (as discussed in the introduction), for all the experiments hereafter, we used the 7-cell fiber whose lower inner core size allows confinement of light to a higher intensity; thereby, the required spectral broadening is achieved at a lower input energy.

In the first stage, a pulse energy of 140 μJ is launched into a 7-cell Kagome fiber of length 3 m using a mode-matched lens of focal length 50 mm. For all further experiments, we only use the 7-cell fiber instead of the 19-cell fiber. The incoupling end of the fiber is mounted on a metal V-groove and left open in ambient air, while the outcoupling end is capped in a high-pressure gas cell with a 5-mm-thick uncoated CaF_2 window. The GDD introduced from the thick window is of little significance here due to the long pulses. Through the gas cell, the Ar-gas of pressure 5 bar is introduced along the fiber, which is coiled in a diameter of 30–40 cm and lies on the optical table without any special mounting between the coupling ends. Due to the open input end of the fiber, there exists a pressure gradient along the fiber length. The broadened spectrum obtained after the first stage (red) has a 10 dB bandwidth of ∼88 nm, corresponding to a Fourier limited (FL) pulse duration of 250 fs (FWHM). The complete characterization of the broadened spectrum at the output of the second stage can be found in Ref. [47]. The broadened spectrum then passes through a set of two prisms mounted in the Treacy style as shown in Fig. 4 whose apex-to-apex distance is varied for the dispersion scan. The prisms are uncoated and made of silicon (Si) at Brewster-cut of height 25.4 mm and an apex angle of 73.84°. The prism material is chosen such that it adds large negative GDD to the pulse so that the distance between the prisms can be kept low. The distance between the prisms is optimized to achieve the shortest pulse duration corresponding to the broadest spectrum of ∼88 nm from the fiber. This is reached with the prism distance of 1.1 m and a fixed insertion length of 10 mm

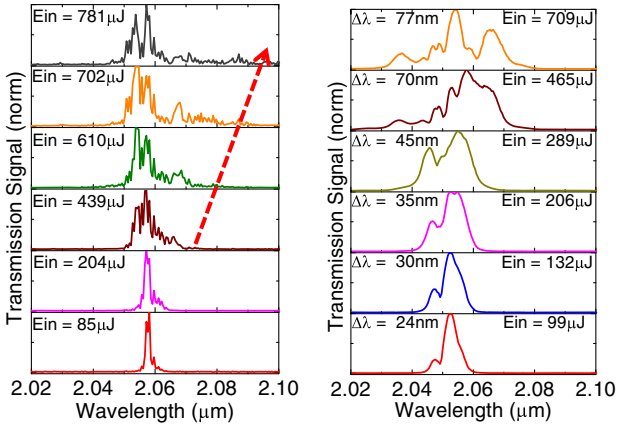

Fig. 3. Measured spectral evolution at the output of the Ar-gas filled 19-cell Kagome fiber at a pressure of 3 bar with an increasing input energy at a pulse duration of 3.3 ps (left) and 1.8 ps (right).

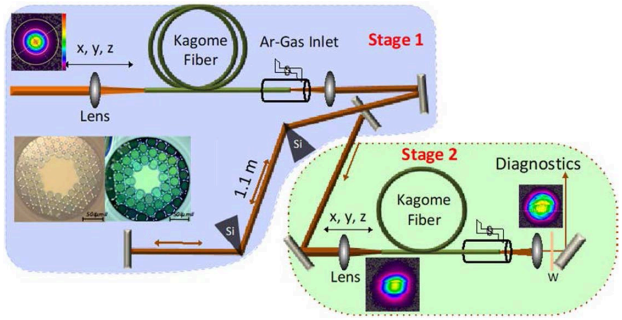

Fig. 4. Experimental layout of the two-stage compression in 7-cell Kagome fiber: the first stage comprises spectral broadening in the fiber of length 3 m and a prism compressor whose tip-to-tip separation is 1.1 m. The output of the first stage is launched in the second piece of Kagome fiber and self-compressed with the outer end placed in the gas cell. The GDD of the thin window of the gas cell is used to compensate for the small positive chirp remaining in the fiber.

introducing a GDD of -1.54×10^5 fs^2. The input energy, gas pressure, and dispersion (prism distance) are chosen after careful optimization for best compression results. The transmission efficiency of the fiber is 85% while that of the compressor is 75% that leads to a compressed energy of 90 μJ. The transmitted energy is chosen as a trade-off between operating the experiment safely without damaging the fiber and a soliton-like pulse at the output with no or limited pre- or post-pulses. The compressed output pulse from the first stage is then launched into the incoupling port of a second piece of 7-cell Kagome fiber of length 80 cm using a focusing lens of 50 mm of focal length while achieving a maximum transmission efficiency of 82%. The second stage arrangement is similar to that of the first stage except that, instead of the external prism compressor to compress the pulse, self-compression is achieved in the fiber due to the interplay between the nonlinearity and the anomalous dispersion of the fiber with an additional thin glass plate to optimize the overall dispersion. The experiment is performed both in presence of air and krypton (Kr) gas at a pressure of 3 bar and 5 bar.

3. RESULTS AND DISCUSSION

A. Pulse Dynamics and Modulation Instability

Though the main mechanism of spectral broadening in PCF is SPM, the dynamics can vary significantly with the input pulse duration and the fiber parameters as different higher-order nonlinear effects can play a crucial role. Broadly, the pulse duration is classified into two regimes: an ultrashort fs-regime and a longer ps-regime. For this reason we divided the experiments into two stages. In the first stage, the pulses are in ps-regime, while in the second stage they are in fs-regime. In particular, the pulse dynamics varies significantly with the position of the input pulse wavelength relative to the zero-dispersion wavelength (ZDW). Regardless of the input pulse duration, when operating in the normal dispersion regime, the spectral broadening in both fs- and ps-regimes is heavily dominated by SPM. However, when operating in anomalous dispersion, in addition to SPM, more complex physics is involved, which is dominated by soliton-related dynamics. Depending on the input peak intensity, either solitonic self-compression occurs or, if the peak intensity is high, soliton fission occurs in which the pulse with sufficient peak power breaks up into a series of lower power sub-pulses due to the perturbation of higher-order dispersion or Raman scattering. The pulse breakup is generally linked to the soliton order (N) related to the dispersion length (L_D) and nonlinear length (L_{NL}) and is given by $N = \sqrt{L_D/L_{\mathrm{NL}}}$. The L_{NL} accounts for SPM while the L_D accounts for the GDD in the fiber; $L_{\mathrm{NL}} = 1/\gamma P_0$, and $L_D = T_0^2/|\beta_2|$, where $\gamma = 2\pi n_2/\lambda A_{\mathrm{eff}}$ is the nonlinear parameter of the fiber, n_2 is the nonlinear refractive index coefficient, λ is the wavelength, T_0 is input pulse duration, and β_2 is the negative GDD of the fiber. In general, pulse breakup into a train of individual pulses via soliton-fission is apparent for $N > 5$, while for $N < 5$ soliton fission can be avoided [49]. Hence, it is important to get the pulse ejected from the fiber before fission occurs. The characteristic length at which soliton fission occurs is defined as $L_{\mathrm{fiss}} \sim L_D/N$. If the fissioned solitons continue to propagate in the fiber and the soliton spectrum overlaps with the Raman gain, soliton self-frequency shift occurs. This leads to a continuous shift of each constituent soliton to a longer wavelength. In the ps-regime, nonlinear compression is much more complex as here the initial pulse dynamics is dominated by modulation instability (MI). MI is parametric amplification of broadband noise due to the FWM process. Although the end result may be similar to that of soliton fission (fs-regime), i.e., breakup into constituent sub-pulses, the difference comes from the fact that here the dynamics is initiated from noise and shot-to-shot fluctuations, while in the case of fission it is initiated by high-order dispersion or nonlinearities. A detailed review on the pulse dynamics in these fibers is given by Dudley *et al.* [49]. It is, hence, important to find the point where the soliton order can be kept low enough while still maintaining enough broadening.

Table 1 summarizes the calculation of the L_{NL}, L_D, and N for air, Ar, and Kr filled PCF at 5 bar pressure. It can be seen that N has a dramatically high value of 134 in case of 3.3 ps. With such a high value of N, the phenomena of MI and high-order effects make the experiments quite challenging as they become highly prone to slightest amount of noise or shot-to-shot fluctuations emanating from the input source. However, we observed experimentally that with the input duration of 1.8 ps, such effects are relatively reduced where N reduces to less than 100 (Fig. 3). With 3.3 ps, we sometimes also observed plasma in the fiber leading to its damage at different pulse energy while this effect was not observed when the input duration was reduced to 1.8 ps.

B. Pulse Characterization

The optical pulses are characterized using a home-built second-harmonic generation-frequency-resolved optical gating (SHG-FROG) setup employing a 200-μm-thick BBO crystal. The results of these measurement can be found in Ref. [47]. The FROG retrieval of the pulses at the output of the first stage yields a duration of 285 fs with the FL of 244 fs. To achieve further compression, the 285 fs pulse obtained from the first stage is launched into the second stage fiber. Since, in the first stage, the ps pulse from the Ho-CPA is reduced to 285 fs and the pulse duration at the input of the second stage is in the fs-regime, the L_D of the fiber is a few meters, making it a preferable choice for self-compression. The pulse energy after the prism compressor of the first stage is 90 μJ. The input energy to the second stage is controlled by the combination of a half-wave plate (HWP) and a thin-film polarizer (TFP). The spectral characteristics of the transmitted pulse as measured with a

Table 1. Calculated Dispersion Length[a], Nonlinear Length[b], Soliton Order[c], at Different Pulse Duration for Air, Ar, and Kr Gas

		Argon-5 bar		Krypton-5 bar		Air-1 atm	
τ (fs)	L_D (m)	L_{NL} (m)	N	L_{NL} (m)	N	L_{NL} (m)	N
3300	4644	0.26	134	0.08	239	1.62	54
1800	1382	0.14	99	0.04	176	0.88	40
285	35	0.03	32	0.01	56	0.22	13

[a] L_D.
[b] L_{NL}.
[c] N.

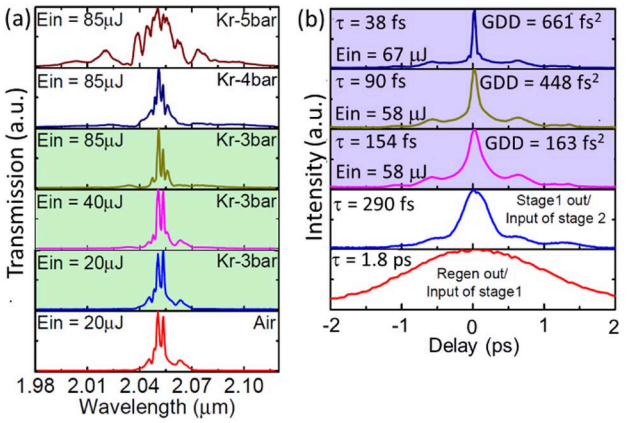

Fig. 5. (a) Measured spectral evolution obtained at the output of the second stage with increasing input pulse energy for three different gas conditions in the fiber: air at 1 atm pressure; Kr gas filled in the fiber at a pressure of 3, 4, and 5 bar. (b) Measured autocorrelation trace at the input of the first stage (red), input of the second stage (blue), output of the second stage (highlighted background) with different amount of negative GDD added to optimize the remaining chirp from the second stage fiber compressor.

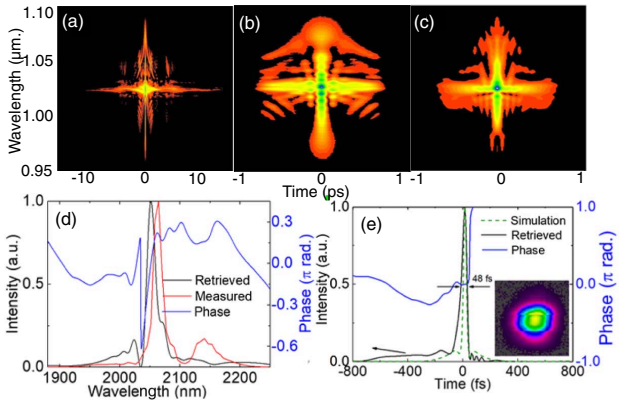

Fig. 6. FROG results of output pulse from the second stage based on 7-cell Kagome fiber of length 2 m filled with air. (a) Measured FROG trace shown on the full time scale; (b) FROG trace after filtering out the compressed part using a super-Gaussian filter in the time domain; (c) reconstructed FROG trace retrieved from the filtered trace; (d) measured (red) and retrieved (black) spectrum with the retrieved spectral phase in blue; (e) retrieved temporal profile (black) and retrieved temporal phase (blue) overlaid with the simulated profile in the green dotted line.

mid-IR spectrometer for different input pulse energies and gas pressure are shown in Fig. 5(a). Initially, at a pulse energy of 20 μJ, almost no spectral broadening is observed regardless of the presence of air or Kr gas at 3 bar pressure. With an increase in pulse energy to 40 μJ and 85 μJ at the same gas pressure, still, no broadening is observed. However, as the gas pressure is increased from 3 bar to 5 bar, broadening is observed. With a gas pressure of 5 bar and an input energy of 85 μJ, a 10 dB bandwidth of ∼370 nm is obtained. We repeated the experiment in air after changing the fiber length from 80 cm to 2 m, whose autocorrelation results obtained at the output of the second stage are shown in Fig. 5(b). With 58 μJ of input pulse energy, an output duration of 154 fs is obtained. The residual chirp is compensated by adding a thin sapphire plate of 3 mm that exhibits negative GDD at this wavelength. The autocorrelation results indicate that, by adding negative GDD of −163 fs^2, −468 fs^2, and −611 fs^2, the pulse can be compressed to 154 fs, 90 fs, and 38 fs, respectively, in addition to the GDD introduced by the 2 mm thin CaF_2 window present in the gas cell.

The shortest output pulse with the autocorrelation value of 38 fs obtained in the presence of air is then characterized using the FROG, and the results are shown in Fig. 6. Figure 6(a) shows the measured FROG trace shown on full time scale while Fig. 6(b) shows the trace after filtering out the compressed part using super-Gaussian filter in the time domain where about 28% of the entire pulse energy is contained. This is done to avoid the numerical issues emerging from the high complexities of the FROG trace data between the long ps pulse in the background and the ultrashort component. The reconstructed FROG trace of the filtered trace in Fig. 6(b) is shown in Fig. 6(c). From the reconstruction, we obtain a 48 fs FWHM duration of the compressed component that contains 67% (−100 fs to 300 fs) of the pulse energy. Thus, overall the compressed part contains 28% × 67% = 19% of the total output pulse energy of 60 μJ, i.e., 11 μJ of 48 fs centered at 2060 nm is obtained. Figure 6(d) shows the retrieved spectrum (black) and its spectral phase (blue) together with the measured spectrum (red) that matches well. Figure 6(e) shows the retrieved temporal intensity profile (solid black line) and the FL profile (dotted red line) calculated from the independently measured spectrum with the temporal phase in blue. The overlaid green dotted line in Fig. 6(e) is the simulated profile.

Finally, we measure the pulse-to-pulse power stability of the overall system using a thermal powermeter PM10 from Coherent Inc. The output power from the second stage is directed to the powermeter, and simultaneously we measure the fluctuations from the Ho-CPA. Figure 7(a) shows the power stability measured at the output of the second stage (red) and from the amplifier (black) for 70 min with a root mean square deviation value of 0.22% and 0.42%, respectively. The amplifier is operated under humidity level <2%, and the first stage fiber is filled with Ar pressure of 5 bar. It is worth noting that the output power of 60 mW and pulse duration of 48 fs were also stable over a duration of 24 h operation. Figure 7(b) shows the combined spectrum at the input of the first stage

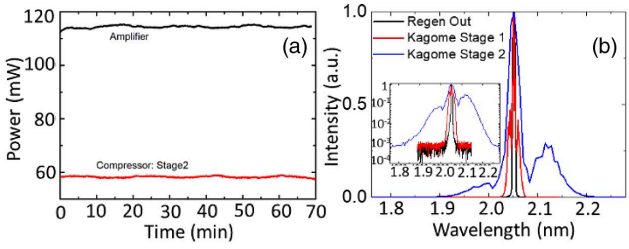

Fig. 7. (a) Measured pulse-to-pulse fluctuations for 70 min at the output of the Ho-CPA (black) and after the second stage compression (red); (b) measured output spectra from the amplifier (black), after compression from the first stage Kagome fiber (red) and from the second stage Kagome fiber (blue).

(black) and second stage (red) while the output of the second stage is shown in blue.

C. Simulation

To understand the compression dynamics in the second stage Kagome fiber operated at 2 μm, we simulated the nonlinear pulse propagation in HC-PCF using a numerical model based on a 1D nonlinear Schrödinger equation given by

$$i\frac{\partial A}{\partial z} = \frac{\beta_2}{2}\frac{\partial^2 A}{\partial t^2} - \gamma|A|^2 A - i\frac{\gamma}{\omega_0}\frac{\partial}{\partial t}(|A|^2 A). \quad (1)$$

Here, the term γ is a constant nonlinear parameter and has a value of 5.9×10^{-8} mW^{-1} while ω_0 is the central angular frequency. The numerical code includes SPM and self-steepening. Due to relatively lower peak intensity level in the fiber, we exclude the photoionization/plasma term and higher-order effects. The linear second-order dispersion term β_2 is added as a constant factor including the geometric dispersion of the 7-cell fiber with a value of −2345 fs^2/m. The gas pressure is assumed static throughout the fiber. The simulation is performed using the split-step Fourier transform technique and is first benchmarked with the experimental data of the first stage. We used the experimentally measured spectrum obtained at the input of the first stage for simulating the propagation of the optical pulse along the 7-cell fiber of 3 m length in the presence of Ar in the first stage compression. Both the simulated output temporal and spectral profiles match well with the results obtained experimentally [47]. After benchmarking the code, the output spectrum obtained from the first stage is used as an input to the second stage, and the pulse is simulated again. The simulations are performed with a different fiber length and input energy, and we found that pulse compression is best achieved around the fiber length of 2–2.5 m. Beyond this length, pulse splitting occurs. This helped us in choosing the approximate length of the fiber. However, to be able to match well the spectra and the temporal profile of experiment, the simulations had to be performed with lower input energy of 73 μJ, while the experiment is performed at an input energy of 90 μJ. Thus, mismatch is common in these experiments that might arise from discrepancies in the parameters used from the literature such as nonlinear index. Also, the long pedestal as obtained in experiment is not seen in the simulation, which might come from the higher-order effects, which is the limitation of our simulation. The results obtained are shown in Figs. 8(a) and 8(b). It shows the temporal and spectral profile, respectively, obtained as the pulse propagates along the fiber length. Figure 8(c) shows the simulated and the measured spectrum while Fig. 8(d) shows the corresponding temporal intensity profile at the end of the fiber.

D. White Light Generation Using 48 fs, 2 μm Pulses

The output pulse obtained after the second Kagome fiber stage is focused by an AR-coated lens of 50 mm focal length into a 3 mm thin YAG plate. Figure 9 shows the images of the generated white light captured with a camera for different input energy and the schematic of the setup. The input pulse energy is increased in steps from 10 μJ to 60 μJ in the energy increments of 10 μJ. The input energy is controlled using a TFP and an HWP.

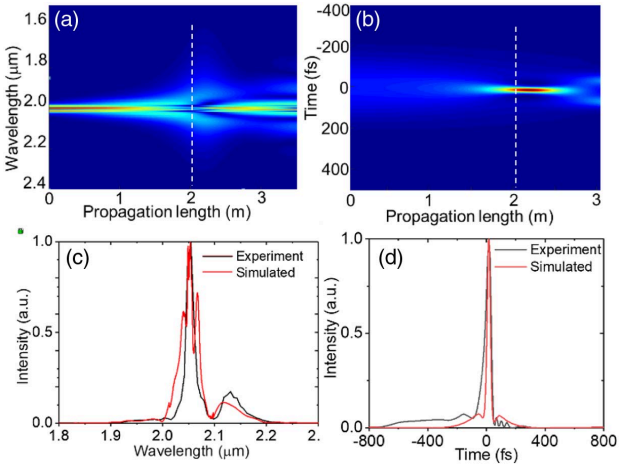

Fig. 8. Simulation results after the second stage with a fiber length of 2 m and input pulse parameters obtained from the output of the first stage. (a) Spectral evolution along the fiber length; (b) temporal evolution along the fiber length, the white dashed line indicates the pulse exit point from the fiber; (c) simulated spectrum (red); (d) simulated temporal profile (red) obtained at the end of the fiber length, overlaid with the experimental profile (black).

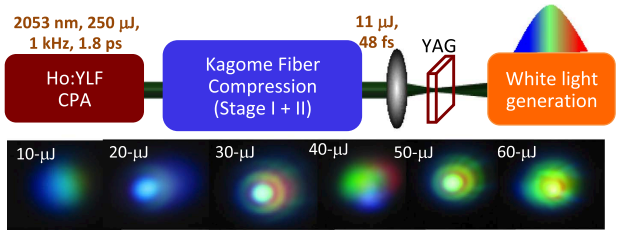

Fig. 9. White light generation in a thin YAG plate with pulses derived from the two-stage Kagome compressor for different input energies. The top panel shows the schematic of white light generation setup.

4. CONCLUSION

In summary, the Ho-CPA operates at 1 kHz repetition rate and delivers pulses at the mJ level and with durations in the few ps range. A small portion of the output energy is spectrally broadened in a first stage Kagome fiber and compressed using a silicon (Si) prism pair. With an input pulse energy of 140 μJ, the pulses are compressed to 285 fs with an output energy of 90 μJ. The output pulse is further spectrally broadened and self-compressed in a second stage air-filled Kagome fiber of 2 m length leading to pulse duration of 150 fs. With proper GDD compensation using a thin sapphire window of 3 mm, output pulses of 48 fs duration are obtained with a pulse energy of 60 μJ and 19% of the energy, i.e., 11 μJ, in the main peak. After compression of the picosecond pulses down to 48 fs in a two-stage Kagome compressor at 2 μm wavelength, we also generated white light with this compressed pulse that confirms the coherent nature of the compressed pulse and suitability for experiments. With only 140 μJ of energy used for compression, the system as envisioned in Fig. 1 allows pumping of the OPA with

more than 2 mJ of energy. When focused to a spot size of 50 μm, the intensity of the output from the second stage can reach peak values of 10^{13} W/cm^2 and, hence, can be directly used for HHG in solids at 2 μm wavelength.

Funding. European Research Council (609920); Hamburg Centre for Ultrafast Imaging; Deutsche Forschungsgemeinschaft; Gordon and Betty Moore Foundation; Agence Nationale de la Recherche; Conseil Régional du Limousin.

Acknowledgment. We thank Oliver D. Mücke for helpful discussions in FROG reconstruction.

Disclosures. The authors declare no conflicts of interest.

Data Availability. Data underlying the results presented in this paper are not publicly available at this time but may be obtained from the authors upon reasonable request.

REFERENCES

1. H. Pires, M. Baudisch, D. Sanchez, M. Hemmer, and J. Biegert, "Ultrashort pulse generation in the mid-IR," Prog. Quantum Electron. **43**, 1–30 (2015).
2. I. Jovanovic, G. Xu, and S. Wandel, "Mid-infrared laser system development for dielectric laser accelerators," Phys. Procedia **52**, 68–74 (2014).
3. H. R. Reiss, "Limits on tunneling theories of strong-field ionization," Phys. Rev. Lett. **101**, 043002 (2008).
4. S. Woutersen, U. Emmerichs, and H. J. Bakker, "Femtosecond mid-IR pump-probe spectroscopy of liquid water: evidence for a two-component structure," Science **278**, 658–660 (1997).
5. A. H. Chin, J. M. Bakker, and J. Kono, "Ultrafast electroabsorption at the transition between classical and quantum response," Phys. Rev. Lett. **85**, 3293–3296 (2000).
6. S. Ghimire, A. D. DiChiara, E. Sistrunk, U. B. Szafruga, P. Agostini, L. F. DiMauro, and D. A. Reis, "Redshift in the optical absorption of ZnO single crystals in the presence of an intense midinfrared laser field," Phys. Rev. Lett. **107**, 167407 (2011).
7. S. Ghimire, A. D. DiChiara, E. Sistrunk, P. Agostini, L. F. DiMauro, and D. A. Reis, "Observation of high-order harmonic generation in a bulk crystal," Nat. Phys. **7**, 138–141 (2011).
8. O. D. Mücke, "Isolated high-order harmonics pulse from two-color-driven Bloch oscillations in bulk semiconductors," Phys. Rev. B **84**, 081202 (2011).
9. G. J. Stein, P. D. Keathley, P. Krogen, H. Liang, J. P. Siqueira, C.-L. Chang, C.-J. Lai, K.-H. Hong, G. M. Laurent, and F. X. Kärtner, "Water-window soft X-ray high-harmonic generation up to the nitrogen K-edge driven by a kHz, 2.1 μm OPCPA source," J. Phys. B **49**, 155601 (2016).
10. J. Pupeikis, P.-A. Chevreuil, N. Bigler, L. Gallmann, C. R. Phillips, and U. Keller, "Water window soft X-ray source enabled by a 25 W few-cycle 22 μm OPCPA at 100 kHz," Optica **7**, 168–171 (2020).
11. X. Ren, J. Li, Y. Yin, K. Zhao, A. Chew, Y. Wang, S. Hu, Y. Cheng, E. Cunningham, Y. Wu, M. Chini, and Z. Chang, "Attosecond light sources in the water window," J. Opt. **20**, 023001 (2018).
12. A. D. Shiner, C. Trallero-Herrero, N. Kajumba, H.-C. Bandulet, D. Comtois, F. Légaré, M. Giguère, J.-C. Kieffer, P. B. Corkum, and D. M. Villeneuve, "Wavelength scaling of high harmonic generation efficiency," Phys. Rev. Lett. **103**, 073902 (2009).
13. M. B. Gaarde, K. J. Schafer, A. Heinrich, J. Biegert, and U. Keller, "Large enhancement of macroscopic yield in attosecond pulse train–assisted harmonic generation," Phys. Rev. A **72**, 013411 (2005).
14. F. Brizuela, C. M. Heyl, P. Rudawski, D. Kroon, L. Rading, J. M. Dahlström, J. Mauritsson, P. Johnsson, C. L. Arnold, and A. L'Huillier, "Efficient high-order harmonic generation boosted by below-threshold harmonics," Sci. Rep. **3**, 1410 (2013).
15. G. Orlando, P. P. Corso, E. Fiordilino, and F. Persico, "A three-colour scheme to generate isolated attosecond pulses," J. Phys. B **43**, 025602 (2010).
16. A. Heinrich, W. Kornelis, M. P. Anscombe, C. P. Hauri, P. Schlup, J. Biegert, and U. Keller, "Enhanced VUV-assisted high harmonic generation," J. Phys. B **39**, S275–S281 (2006).
17. Z. Chang, "Enhancing keV high harmonic signals generated by long-wave infrared lasers," OSA Continuum **2**, 2131–2136 (2019).
18. H. Du, L. Luo, X. Wang, and B. Hu, "Attosecond ionization control for broadband supercontinuum generation using a weak 400 nm few-cycle controlling pulse," Opt. Express **20**, 27226–27241 (2012).
19. T. Popmintchev, M.-C. Chen, D. Popmintchev, P. Arpin, S. Brown, S. Alisauskas, G. Andriukaitis, T. Balciunas, O. D. Mucke, A. Pugzlys, A. Baltuska, B. Shim, S. E. Schrauth, A. Gaeta, C. Hernandez-Garcia, L. Plaja, A. Becker, A. Jaron-Becker, M. M. Murnane, and H. C. Kapteyn, "Bright coherent ultrahigh harmonics in the keV X-ray regime from mid-infrared femtosecond lasers," Science **336**, 1287–1291 (2012).
20. S. Hädrich, M. Krebs, A. Hoffmann, A. Klenke, J. Rothhardt, J. Limpert, and A. Tünnermann, "Exploring new avenues in high repetition rate table-top coherent extreme ultraviolet sources," Light Sci. Appl. **4**, e320 (2015).
21. P. Malevich, G. Andriukaitis, T. Flöry, A. J. Verhoef, A. Fernández, S. Ališauskas, A. Pugžlys, A. Baltuška, L. H. Tan, C. F. Chua, and P. B. Phua, "High energy and average power femtosecond laser for driving mid-infrared optical parametric amplifiers," Opt. Lett. **38**, 2746–2749 (2013).
22. C. R. Phillips, J. Jiang, C. Mohr, A. C. Lin, C. Langrock, M. Snure, D. Bliss, M. Zhu, I. Hartl, J. S. Harris, M. E. Fermann, and M. M. Fejer, "Widely tunable midinfrared difference frequency generation in orientation-patterned GaAs pumped with a femtosecond Tm-fiber system," Opt. Lett. **37**, 2928–2930 (2012).
23. D. Brida, M. Marangoni, C. Manzoni, S. De Silvestri, and G. Cerullo, "Two-optical-cycle pulses in the mid-infrared from an optical parametric amplifier," Opt. Lett. **33**, 2901–2903 (2008).
24. V. Shumakova, P. Malevich, S. Ališauskas, A. Voronin, A. M. Zheltikov, D. Faccio, D. Kartashov, A. Baltuška, A. Pugzlys, and A. Pugžlys, "Multi-millijoule few-cycle mid-infrared pulses through nonlinear self-compression in bulk," Nat. Commun. **7**, 12877 (2016).
25. M. Seidel, G. Arisholm, J. Brons, V. Pervak, and O. Pronin, "All solid-state spectral broadening: an average and peak power scalable method for compression of ultrashort pulses," Opt. Express **24**, 9412–9428 (2016).
26. K. Fritsch, M. Poetzlberger, V. Pervak, J. Brons, and O. Pronin, "All-solid-state multipass spectral broadening to sub-20 fs," Opt. Lett. **43**, 4643–4646 (2018).
27. M. Ueffing, S. Reiger, M. Kaumanns, V. Pervak, M. Trubetskov, T. Nubbemeyer, and F. Krausz, "Nonlinear pulse compression in a gas-filled multipass cell," Opt. Lett. **43**, 2070–2073 (2018).
28. V. Cardin, N. Thiré, S. Beaulieu, V. Wanie, F. Légaré, and B. E. Schmidt, "0.42 TW 2-cycle pulses at 1.8 μm via hollow-core fiber compression," Appl. Phys. Lett. **107**, 181101 (2015).
29. G. Fan, T. Balčiūnas, T. Kanai, T. Flöry, G. Andriukaitis, B. E. Schmidt, F. Légaré, and A. Baltuška, "Hollow-core-waveguide compression of multi-millijoule CEP-stable 3.2 μm pulses," Optica **3**, 1308–1311 (2016).
30. M. Nisoli, S. De Silvestri, and O. Svelto, "Generation of high energy 10 fs pulses by a new pulse compression technique," Appl. Phys. Lett. **68**, 2793–2795 (1996).
31. B. Debord, F. Amrani, L. Vincetti, F. Gérôme, and F. Benabid, "Hollow-core fiber technology: the rising of 'gas photonics'," Fibers **7**, 16 (2019).
32. F. Benabid and P. J. Roberts, "Linear and nonlinear optical properties of hollow core photonic crystal fiber," J. Mod. Opt. **58**, 87–124 (2011).
33. Y. Y. Wang, N. V. Wheeler, F. Couny, P. J. Roberts, and F. Benabid, "Low loss broadband transmission in hypocycloid-core Kagome hollow-core photonic crystal fiber," Opt. Lett. **36**, 669–671 (2011).
34. F. Couny, F. Benabid, P. J. Roberts, P. S. Light, and M. G. Raymer, "Generation and photonic guidance of multi-octave optical-frequency combs," Science **318**, 1118–1121 (2007).

35. Y. Y. Wang, X. Peng, M. Alharbi, C. F. Dutin, T. D. Bradley, F. Gérôme, M. Mielke, T. Booth, and F. Benabid, "Design and fabrication of hollow-core photonic crystal fibers for high-power ultrashort pulse transportation and pulse compression," Opt. Lett. **37**, 3111–3113 (2012).
36. B. Debord, M. Alharbi, L. Vincetti, A. Husakou, C. Fourcade-Dutin, C. Hoenninger, E. Mottay, F. Gérôme, and F. Benabid, "Multi-meter fiber-delivery and pulse self-compression of milli-Joule femtosecond laser and fiber-aided laser-micromachining," Opt. Express **22**, 10735–10746 (2014).
37. B. Debord, M. Maurel, F. Gerome, L. Vincetti, A. Husakou, and F. Benabid, "Strong nonlinear optical effects in micro-confined atmospheric air," Photon. Res. **7**, 1134–1141 (2019).
38. H. Ren, A. Nazarkin, J. Nold, and P. S. Russell, "Quasi-phase-matched high harmonic generation in hollow core photonic crystal fibers," Opt. Express **16**, 17052–17059 (2008).
39. O. H. Heckl, C. R. E. E. Baer, C. Kränkel, S. V. Marchese, F. Schapper, M. Holler, T. Südmeyer, J. S. Robinson, J. W. G. G. Tisch, F. Couny, P. Light, F. Benabid, and U. Keller, "High harmonic generation in a gas-filled hollow-core photonic crystal fiber," Appl. Phys. B **97**, 369–373 (2009).
40. F. Emaury, C. F. Dutin, C. J. Saraceno, M. Trant, O. H. Heckl, Y. Y. Wang, C. Schriber, F. Gerome, T. Südmeyer, F. Benabid, and U. Keller, "Beam delivery and pulse compression to sub-50 fs of a mode-locked thin-disk laser in a gas-filled Kagome-type HC-PCF fiber," Opt. Express **21**, 4986–4994 (2013).
41. O. H. Heckl, C. J. Saraceno, C. R. E. Baer, T. Südmeyer, Y. Y. Wang, Y. Cheng, F. Benabid, and U. Keller, "Temporal pulse compression in a xenon-filled Kagome-type hollow-core photonic crystal fiber at high average power," Opt. Express **19**, 19142–19149 (2011).
42. K. F. Mak, M. Seidel, O. Pronin, M. H. Frosz, A. Abdolvand, V. Pervak, A. Apolonski, F. Krausz, J. C. Travers, and P. S. J. Russell, "Compressing μJ-level pulses from 250 fs to sub-10 fs at 38-MHz repetition rate using two gas-filled hollow-core photonic crystal fiber stages," Opt. Lett. **40**, 1238–1241 (2015).
43. S. Hädrich, M. Kienel, M. Müller, A. Klenke, J. Rothhardt, R. Klas, T. Gottschall, T. Eidam, A. Drozdy, P. Jójárt, Z. Várallyay, E. Cormier, K. Osvay, A. Tünnermann, and J. Limpert, "Energetic sub-2-cycle laser with 216 W average power," Opt. Lett. **41**, 4332–4335 (2016).
44. T. Balciunas, C. Fourcade-Dutin, G. Fan, T. Witting, A. A. Voronin, A. M. Zheltikov, F. Gerome, G. G. Paulus, A. Baltuska, and F. Benabid, "A strong-field driver in the single-cycle regime based on self-compression in a kagome fibre," Nat. Commun. **6**, 6117 (2015).
45. S. A. Mousavi, H. C. H. Mulvad, N. V. Wheeler, P. Horak, J. Hayes, Y. Chen, T. D. Bradley, S. Alam, S. R. Sandoghchi, E. N. Fokoua, D. J. Richardson, and F. Poletti, "Nonlinear dynamic of picosecond pulse propagation in atmospheric air-filled hollow core fibers," Opt. Express **26**, 8866–8882 (2018).
46. A. Benoît, B. Beaudou, M. Alharbi, B. Debord, F. Gérôme, F. Salin, and F. Benabid, "Over-five octaves wide Raman combs in high-power picosecond-laser pumped H_2-filled inhibited coupling Kagome fiber," Opt. Express **23**, 14002–14009 (2015).
47. K. Murari, G. J. Stein, H. Cankaya, B. Debord, F. Gérôme, G. Cirmi, O. D. Mücke, P. Li, A. Ruehl, I. Hartl, K.-H. Hong, F. Benabid, and F. V. X. Kärtner, "Kagome-fiber-based pulse compression of mid-infrared picosecond pulses from a Ho:YLF amplifier," Optica **3**, 816–822 (2016).
48. K. Murari, H. Cankaya, P. Kroetz, G. Cirmi, P. Li, A. Ruehl, I. Hartl, and F. X. Kärtner, "Intracavity gain shaping in millijoule-level, high gain Ho:YLF regenerative amplifiers," Opt. Lett. **41**, 1114–1117 (2016).
49. J. M. Dudley, G. Genty, and S. Coen, "Supercontinuum generation in photonic crystal fiber," Rev. Mod. Phys. **78**, 1135–1184 (2006).